



Super-efficient Electron Acceleration by an Isolated Magnetic Reconnection

H. S. Fu¹, Y. Xu¹, A. Vaivads², and Y. V. Khotyaintsev²

¹ School of Space and Environment, Beihang University, Beijing, People's Republic of China; huishanf@gmail.com

² Swedish Institute of Space Physics, Uppsala, Sweden

Received 2018 November 28; revised 2018 December 15; accepted 2018 December 20; published 2019 January 14

Abstract

Magnetic reconnection—the process typically lasting for a few seconds in space—is able to accelerate electrons. However, the efficiency of the acceleration during such a short period is still a puzzle. Previous analyses, based on spacecraft measurements in the Earth's magnetotail, indicate that magnetic reconnection can enhance electron fluxes up to 100 times. This efficiency is very low, creating an impression that magnetic reconnection is not good at particle acceleration. By analyzing Cluster data, we report here a remarkable magnetic reconnection event during which electron fluxes are enhanced by 10,000 times. Such acceleration, 100 times more efficient than those in previous studies, is caused by the betatron mechanism. Both reconnection fronts and magnetic islands contribute to the acceleration, with the former being more prominent.

Key words: acceleration of particles – magnetic reconnection

1. Introduction

One of the most important abilities of magnetic reconnection—the process of “breaking” and “reconnecting” magnetic field lines in a thin current sheet (Figure 1(a))—is that it can accelerate electrons (Hoshino et al. 2001; Drake et al. 2006; Fu et al. 2006; Pritchett 2006; Hoshino 2012; Guo et al. 2014, 2015; Matsumoto et al. 2015; Li et al. 2018a, 2018b). For many years, this ability has been considered as the main reason responsible for the energetic electrons in solar flares (Lin et al. 2003), magnetospheric substorms (Angelopoulos et al. 2008), and laboratory plasmas (Ji et al. 1998), and consequently the disastrous environment in near-Earth space that can damage spacecraft and injure astronauts. However, because the magnetic reconnection typically occurs in an explosive manner in space and laboratory plasmas within a few seconds (Ji et al. 1998; Burch et al. 2016; Fu et al. 2017), the efficiency of the acceleration during such a short period remains unknown. In other words, is this short-time process sufficient to account for the energetic electrons in space? To solve this puzzle, either a direct investigation of the energy gain (δE) of electrons during reconnection, or an indirect investigation of the electron-flux enhancement (δF), which is a proxy of acceleration based on the assumption that there are more low-energy electrons than high-energy electrons in phase space, is necessary. The previous investigation of this issue, based on spacecraft measurements of magnetic reconnection in the Earth's magnetotail, indicates that such process can enhance electron fluxes (δF) up to 100 times (see Table 1 in Appendix A), either near the reconnection X-line (Øieroset et al. 2002; Imada et al. 2007; Chen et al. 2008; Retinò et al. 2008; Wang et al. 2010; Egedal et al. 2012; Huang et al. 2012; Zhou et al. 2016) or in the reconnection downstream region (Ashour-Abdalla et al. 2011; Fu et al. 2011, 2013a, 2014; Vaivads et al. 2011; Wu et al. 2013; Duan et al. 2014; Lu et al. 2016; Gabrielse et al. 2016; Grigorenko et al. 2016; Liu et al. 2017a, 2017b; Xu et al. 2018a). Obviously, this acceleration efficiency is low, creating the impression that magnetic reconnection is not good at particle acceleration, particularly when compared with that in the radiation belts, where electron fluxes can be enhanced by 10000 times (Thorne et al. 2013).

2. Observations

Here we report a remarkable magnetic reconnection event, during which super-efficient electron acceleration (with flux enhancement up to 10000 times) happens. This event was detected by the Cluster mission (Escoubet et al. 2001) on 2005 October 3, at 11:23 UT, when the spacecraft was located in the Earth's magnetotail at $(-14.8, 5.3, -0.7) R_E$ (see Figure 3(a)). This event is unique and very suitable for addressing the electron acceleration during reconnection for the following two reasons.

First, this is an isolated magnetic reconnection event lasting only 3 minutes (11:22–11:25 UT, see Figure 2(a)). Before the reconnection, from 11:08 to 11:21 UT, the plasma sheet (or current sheet) is very quiet, with no disturbance in magnetic field and flow velocity (see Figures 2(a) and (c)). After the reconnection, the plasma sheet is also very quiet until 11:27 UT (Figures 2(a)–(c)). Such an isolated event indicates that the electron acceleration in this event—if it exists—should be 100 percent attributed to magnetic reconnection, with no contamination by other processes. The super-quiet plasma sheet before reconnection indicates that the electrons are not pre-accelerated; it also indicates that such electrons can be uniform over a long distance in the current sheet (Figure 1(b)), and therefore, the electrons measured by C1 and C3 at the current sheet center are generally the same as that at the “x” point—a place going to host the reconnection process (see Figure 1(b)).

Second, the four Cluster probes formed a multi-scale configuration in this event (see Figure 3(a)), with C1 and C3 always at the current sheet center and C2 first at the current sheet center but later during reconnection moving to the plasma lobe (see Figures 1(b)–(c) and the B_x component in Figure 3(b)). This enables a comprehensive view of the electron acceleration during reconnection. Specifically, both the plasma-sheet and plasma-lobe electrons can participate in the reconnection, thus both populations can be accelerated (Vaivads et al. 2011). If the plasma-sheet electrons are accelerated, C1 and C3 will measure the source at the center of a quiet current sheet (Figure 1(b)) and the result in the reconnection outflow region (Figure 1(c)). If the plasma-lobe electrons are accelerated, C2 will measure the source in the

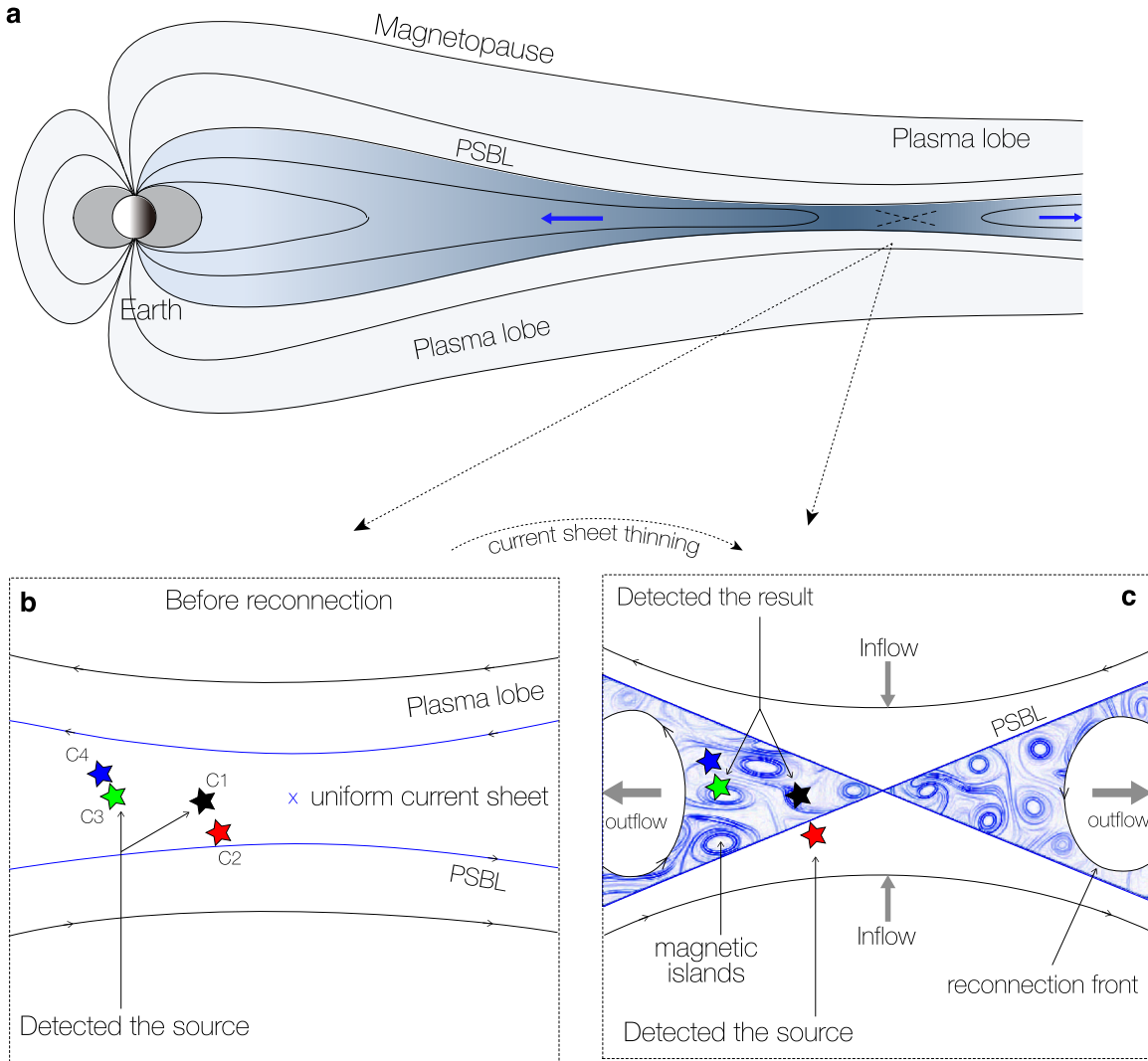


Figure 1. Schematic of electron acceleration during magnetic reconnection. (a) The Earth’s magnetosphere in the noon-midnight plane, showing the convergence of magnetic field lines. The stretched shade describes a current sheet, which is also known as a plasma sheet due to the high plasma density. The white area surrounding the plasma sheet is the plasma lobe, inside which the plasma density is low. Between the plasma sheet and the plasma lobe is the “plasma sheet boundary layer” (PSBL). (b) A close-up view of the current sheet before reconnection. Such a current sheet is very quiet, significantly stretched, and uniform over a long distance. In this sense, the electron population measured by C1 and C3 at the current sheet center is generally same as that at the “x” point—the place where the reconnection process is hosted. The black, red, green, and blue stars denote the four Cluster probes, C1-C4, respectively. (c) A close-up view of the current sheet during reconnection. Such a reconnection is driven by the current sheet thinning. Owing to the time-dependent inflow velocity, magnetic reconnection is unsteady (Fu et al. 2013a), and consequently a pair of reconnection fronts is formed (Fu et al. 2013b). Magnetic islands are also formed (Fu et al. 2013a). All of these reconnection signatures, including current sheet thinning, magnetic islands, and reconnection fronts, are observed in this event. During reconnection, low-energy electrons are convected to the inflow region, accelerated near the X-line, and then ejected in the outflow region (Wei et al. 2007; Cao et al. 2017; Peng et al. 2017). To quantify the acceleration, C1 and C3 measure the source at the center of a quiet uniform plasma sheet (b) and the result in the outflow region (c); C2 measures the source in the inflow plasma-lobe region (c). The reconnection front was first detected by C3 then by C1, because C3 captured a fast flow channel, while C1 captured a slow flow channel (see Appendix II).

inflow region (Figure 1(c)), and again C1 and C3 measure the result in the outflow region (Figure 1(c)).

Being aware of these two unique characteristics, we are able to analyze the electron acceleration during reconnection. We notice that the reconnection signature in this event is clear, although Cluster did not cross the diffusion region. Particularly, the reconnection fronts detected by C1 and C3, with the sudden increase of magnetic field B_z from 0 to 15 nT (Figures 2(d) and (e)), and the magnetic islands exhibiting bipolar variations of B_z from -10 nT to $+10$ nT (Figures 2(d) and (e)), both indicate unsteady magnetic reconnection (Angelopoulos et al. 2013; Fu et al. 2013a, 2013b; Wang et al. 2017; see also the illustration in Figure 1(c)). Such a reconnection is preceded by the current sheet thinning (Figures 1(b) \rightarrow (c)), which was observed during

11:15:47–11:18:50 UT (see the red line in Figure 2(b)). The sudden disturbance of B_x , measured by C2 at 11:21:50 UT (Figure 2(b)), is an indication of the trigger of reconnection (Xu et al. 2018b). Such a disturbance, originating from the X-line and propagating with Alfvén speed, is observed first by C2, because C2 was near the PSBL (see the blue lines in Figures 1(b) and (c)). The velocity of reconnection outflow reaches $V_x = 1200 \text{ km s}^{-1}$ (Figure 2(c)), which is larger than most of those reported in previous studies (Baumjohann et al. 1989; Angelopoulos et al. 1992; Cao et al. 2006, 2013).

In this event, the electron acceleration is indeed observed. Such an acceleration signature is clear in both the measurements of thermal electrons by the Plasma Electron And Current

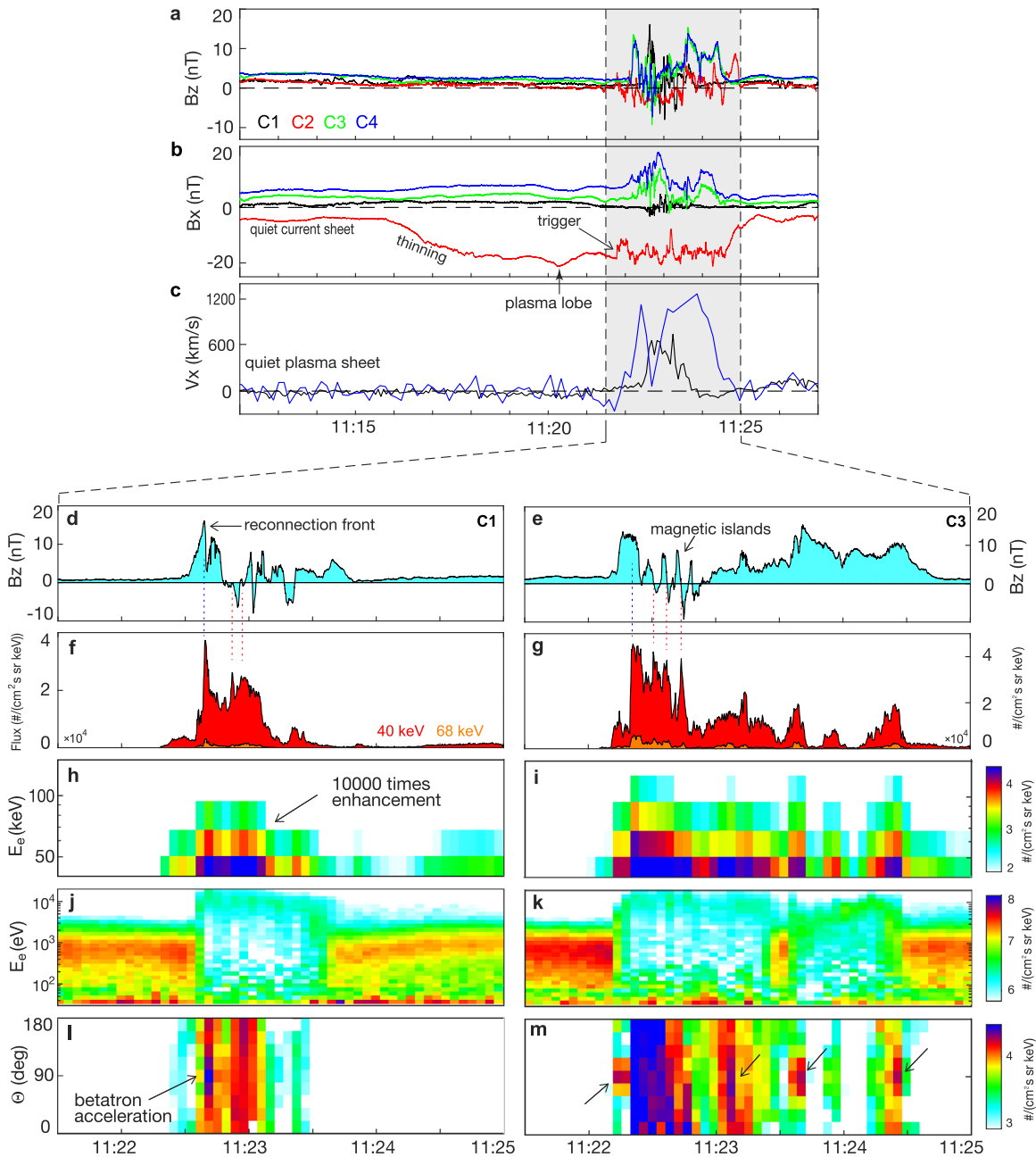


Figure 2. Cluster measurements of electron acceleration during an isolated reconnection event on 2005 October 3. (a–b) The magnetic field B_z and B_x components. (c) The bulk flow velocity V_x component. In (a–c), the black, red, green, and blue lines show the data of C1–C4, respectively. Because the ion velocities measured by C2 and C3 are not available, they are not shown. The gray shade highlights the interval when reconnection happens. A close-up view of this interval is shown in (d–m). Specifically, the left column shows the C1 data, while the right column shows the C3 data. (d–e) The magnetic field B_z component. (f–g) The differential particle flux (DPF) of the 40 and 68 keV electrons at sub-spin resolution. (h–i) The DPF of the 40–176 keV electrons at spin resolution. (j–k) The DPF of the 0.03–20 keV electrons. (l–m) The pitch angle distribution of the 40–68 keV electrons, with an enhancement of DPF around $\theta = 90^\circ$ indicating the betatron acceleration. In (d–e), the sharp increase indicates a reconnection front (Fu et al. 2012a, 2012c; Angelopoulos et al. 2013; Yang et al. 2017; Liu et al. 2018a, 2018b, 2018c), while the multiple bipolar variations indicate magnetic islands (Drake et al. 2006; Chen et al. 2008), as shown in Figure 1(c). These multiple bipolar variations should not be interpreted as waves, because the flow speed during this period is large. Inside a fast flow, the magnetic fluctuations are usually identified as signatures of spatial structures rather than temporal variations (e.g., Retinò et al. 2007; Phan et al. 2018). In (b), the gradual decrease of B_x from 11:15:47 to 11:18:50 UT is a signature of current sheet thinning (Xu et al. 2018b); the small valley of B_x at 11:20:16 UT indicates that C2 entered into the plasma lobe, because at that time the plasma density significantly dropped (see Figure 3(c)); the sudden disturbance of B_x at 11:21:50 UT indicates the trigger of reconnection. In (a), the reconnection front was first detected by C3 (located earthward) then by C1 (located tailward), because C3 captured a fast flow channel ($V_x = 1200 \text{ km s}^{-1}$) while C1 captured a slow flow channel ($V_x = 600 \text{ km s}^{-1}$; see Appendix II). C2 observed the magnetic islands (a), because during development of magnetic reconnection C2 went back to the outflow region again.

Experiment instrument (PEACE) instrument (Johnstone et al. 1997; Figures 2(j)–(k)) and the measurements of supra-thermal electrons by the Research with Adaptive Particle Imaging Detectors instrument (RAPID; Wilken et al. 1997; Figures 2(f)–(i)). In the PEACE measurements, we find that

the electrons primarily have energy below 2 keV before reconnection in the quiet plasma sheet but have energy above 10 keV in the outflow region after reconnection (Figures 2(j)–(k)). A large portion of electrons have been accelerated beyond the scope of the PEACE instrument during

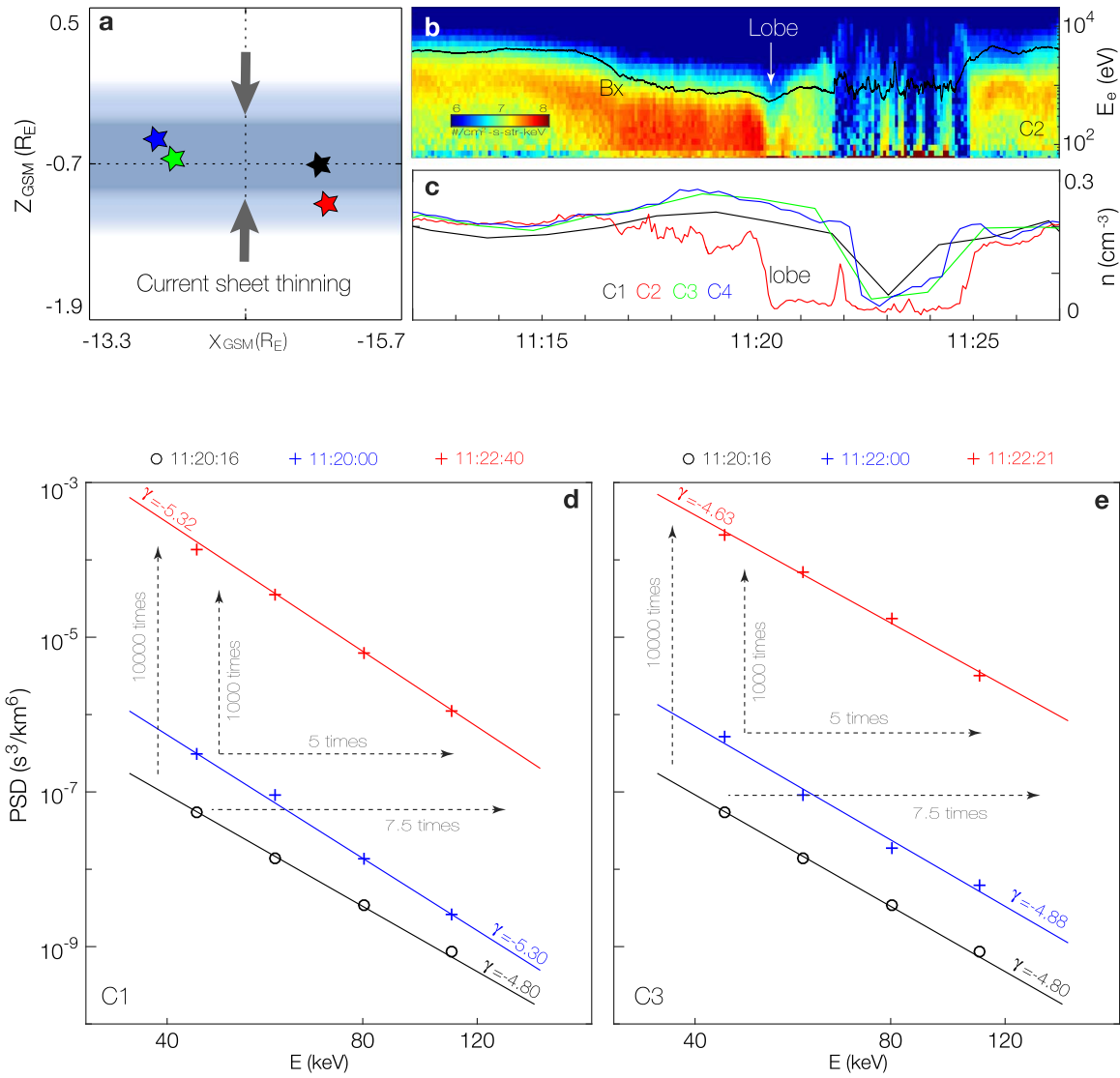


Figure 3. Quantifying the efficiency of electron acceleration during reconnection. (a) Cluster configuration in the XZ plane, with the light-blue belt denoting the thick current sheet before evolution, and the grayish-blue belt denoting the thin current sheet after evolution. (b) The DPF of the 0.03–20 keV electrons and the magnetic field B_x component, measured by C2. At 11:20:16 UT, a tiny disturbance in B_x led to the sharp drop of DPF, suggesting that C2 entered into the plasma lobe and wandered near the PSBL until 11:21:50 UT. (c) The plasma density measured by the PEACE instrument (Johnstone et al. 1997), with the photoelectron contamination removed. Respectively, the black, red, green, and blue lines represent the measurements of C1–C4. (d) C1 measurements of the source population in the quiet current sheet (blue crosses) before reconnection at 11:20:00 UT and resultant population in the outflow region (red crosses) after reconnection at 11:22:40 UT. (e) C3 measurements of the source population in the quiet current sheet (blue crosses) before reconnection at 11:22:00 UT, and the resultant population in the outflow region (red crosses) after reconnection at 11:22:21 UT. In both (d) and (e), the black circles denote the source population measured by C2 in the inflow plasma-lobe region at 11:20:16 UT; the solid lines are the fitting of spacecraft measurements, with γ denoting the slope of the lines—known as the “power-law index”. The vertical arrows show the electron flux enhancement, while the horizontal arrows indicate the energy gain (δE), derived from the Liouville mapping (Egedal et al. 2012). According to Liouville’s theorem, the electron phase space density (PSD) should be conserved during acceleration, and thus we can trace the electron energy before acceleration along a constant PSD to find the electron energy after acceleration. Clearly, during reconnection, the PSD of plasma-lobe electrons is elevated by 10000 times, and correspondingly the electron energy is elevated by 7.5 times.

reconnection, which rarely happened in previous studies. In the RAPID measurements, we find no electrons above 40 keV before reconnection, but many electrons above 150 keV after reconnection (Figures 2(h)–(i)). The sub-spin measurements of the 40 and 68 keV electrons (Figures 2(f)–(g)) also indicate significant enhancement of electron fluxes during reconnection. Because no other processes occurred during this period, the electron acceleration observed here is 100 percent attributed to magnetic reconnection. From the trigger of reconnection at 11:21:50 UT (Figure 2(b)) to the observation of the maximum flux at 11:22:21 UT

(Figure 2(g)) or 11:22:40 (Figure 2(f)), the acceleration takes about 30 seconds.

Apparently, the electron acceleration in this event is efficient, but exactly how efficient is it? To quantify the acceleration efficiency, the source population before reconnection and the resultant population after reconnection should both be observed. If the plasma-sheet electrons are accelerated, the source population should be measured at the center of a quiet current sheet, and the resultant population should be measured in the reconnection outflow region. To satisfy this criterion, we can treat the C1 measurement at 11:20:00 UT and the C3

measurement at 11:22:00 UT as the source, because at these moments C1 and C3 were located at the center of a quiet current sheet (see Figure 1(b) and Figure 2(a)), and treat the C1 measurement at 11:22:40 UT and C3 measurement at 11:22:21 UT as the result, because at these moments C1 and C3 were in the outflow region and measured the maximum electron flux (see Figure 1(c) and Figures 2(f)–(g)). If the plasma-lobe electrons are accelerated, the source population should be measured in the inflow plasma-lobe region, and the resultant population should be measured in the reconnection outflow region. To satisfy this criterion, we treat the C2 measurement at 11:20:16 UT as the source, because at that moment C2 entered into the plasma-lobe region due to the current sheet thinning (see Figure 1(c) and Figures 3(b)–(c)), and once again treat the C1 measurement at 11:22:40 UT and C3 measurement at 11:22:21 UT as the result (see Figure 1(c)).

Figures 3(d)–(e) present the PSD of both the source and resultant populations during acceleration. The PSDs of the plasma-sheet electrons (blue lines) are elevated by 1000 times during reconnection; the PSDs of the plasma-lobe electrons (black lines) are elevated by 10000 times. We use Liouville mapping (Egedal et al. 2010; Liu et al. 2017c) to examine the energy gain (δE) of plasma-sheet electrons and find that it is five times as much (top horizontal arrows). If we perform the Liouville mapping to plasma-lobe electrons, the energy gain can reach 7.5 times as much (bottom horizontal arrows). Because the resultant electrons (C1 measurement at 11:22:40 UT and C3 measurement at 11:22:21 UT) have densities similar to the plasma-lobe population (see Figure 3(c)), it is more likely that the C2 measurement at 11:20:16 UT (in the lobe) is the source population in this event. In this sense, the electron flux enhancement (or PSD increase) in this event should be 10000 times as much, and correspondingly the electron acceleration is 7.5 times as much. Here the flux enhancement (10000 times) and electron acceleration (7.5 times) have no direction relation; in other words, their relation depends on the power-law index. In fact, flux enhancement is just a proxy—but traditionally used in spacecraft measurements—of the electron acceleration, based on the assumption that low-energy electrons are more than high-energy electrons in phase space.

3. Discussion

Such acceleration is super efficient. Compared to the acceleration in previous studies, where the flux enhancement up to 100 times was found (see Table 1 in Appendix A), the electron acceleration in this event is 100 times more efficient. In fact, we have analyzed nine years (2001–2009) of Cluster measurements in the Earth’s magnetotail and found that this event is the most prominent one. The super-efficient electron acceleration in this event is even comparable to that in the radiation belts (Thorne et al. 2013). However, to achieve 10000 times the flux enhancement, it takes more than 16 hr in the radiation belts (Thorne et al. 2013) but only 30 s in this event.

In this event, the electron PSD well follows the power-law distribution (Figures 3(d)–(e)), with an index ranging from $\gamma = -4.63$ to $\gamma = -5.32$. Such power-law indices are similar before and after the reconnection, particularly in the C3 measurements (Figure 3(e)), meaning that the acceleration by reconnection is quasi-adiabatic. We examine the pitch angle distribution of the accelerated electrons and find that it is near

90° (Figures 2(l)–(m), see the arrows). This implies that the betatron mechanism (Fu et al. 2011, 2012b)—an adiabatic process elevating electron speed in the direction perpendicular to magnetic field—takes place during the acceleration. Both the reconnection fronts and magnetic islands contribute to the acceleration (Figures 2(d)–(g)). Specifically, the acceleration by reconnection fronts occurs at the maximum of magnetic field (see the blue dashed lines in Figures 2(d)–(e)), while the acceleration by magnetic islands occurs at the center of such structures ($B_z = 0$, see the red dashed lines in Figures 2(d)–(e)). It seems that the acceleration by reconnection fronts is more efficient than the acceleration by magnetic islands. The maximum electron fluxes that we consider in Figures 3(d)–(e) (C1 measurement at 11:22:40 UT and C3 measurement at 11:22:21 UT) are found exactly at the reconnection fronts. Notice that in Figure 2(l) some isotropic distributions are observed during the low-flux time (11:22:50–11:23:30 UT). These isotropic distributions may be attributed to the pitch angle scattering, which causes electrons to lose energy. Such a scattering process can explain why the electron fluxes associated with isotropic distributions are lower than the electron fluxes associated with pancake distributions (see Figure 2(l)).

The reason why this event is so efficient in electron acceleration is probably the long-time accumulation of magnetic energy before magnetic reconnection. From 11:15:47 to 11:21:50 UT (Figure 2(b)), the current sheet is slowly thinning, and the magnetic energy is slowly accumulated. Such energy accumulation time (6 minutes) is much longer than the electron acceleration time in this event, which is about 30 s (from 11:21:50 to 11:22:21 UT). It will store more magnetic energy in the thin current sheet and finally lead to the explosive release of these energies during reconnection. Unfortunately, we cannot compare the energy accumulation time in this event with the accumulation time in other events, because such accumulation is hard to define in other events. Typically, in other events, multiple processes are involved in addition to the magnetic reconnection, and thus one cannot know when the energy accumulation starts and when the reconnection starts. In this event, however, the magnetic reconnection is very clean and isolated, with no contamination by other processes, so that we can unambiguously define the accumulation time of magnetic energy. In other words, this is a very unique event, particularly suitable for quantifying the acceleration efficiency of magnetic reconnection.

4. Conclusion

In summary, we report a super-efficient electron acceleration during an isolated magnetic reconnection in the Earth’s magnetotail. Such acceleration is probably attributed to the long-time accumulation of magnetic energy before reconnection. This finding has greatly improved our knowledge of magnetic reconnection. It also demonstrates the efficiency of magnetic reconnection as a universal particle-energization process in space.

We thank the Cluster Science Archive for providing the data for this study. This research was supported by NSFC grants 41404133, 41874188, 41574153, 40621003, and 41431071.

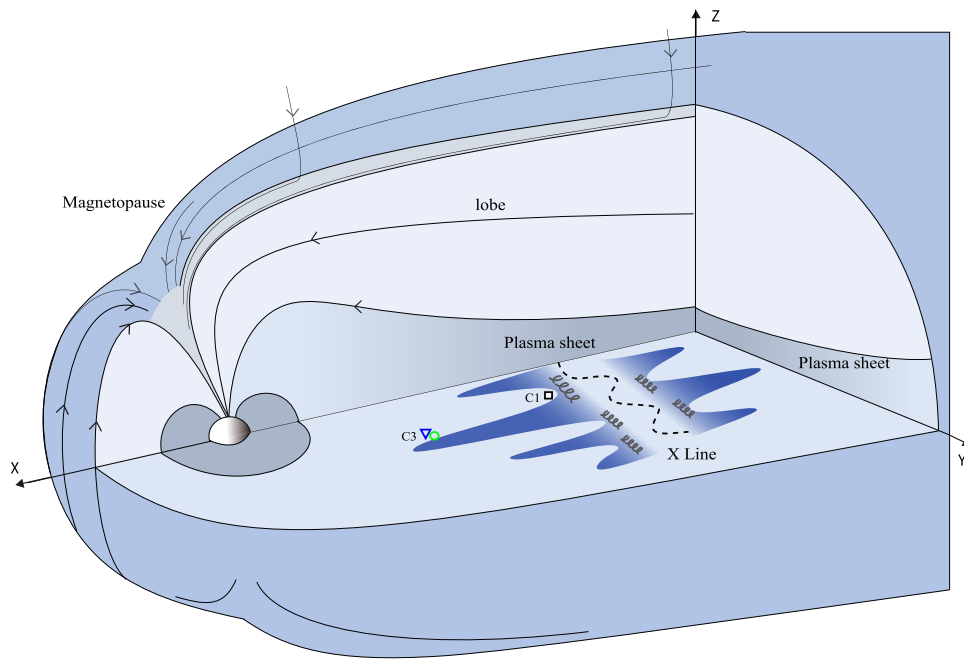


Figure 4. Schematic of reconnection outflow and reconnection front.

Table 1
Summary of Electron Acceleration by Magnetic Reconnection

Research Method	Acceleration Region	Flux Enhancement (F_2/F_1)	References
Statistics	Magnetotail	$F_2/F_1 < 10$	Duan et al. (2014)
Statistics	Magnetotail	$F_2/F_1 < 10$	Zhou et al. (2016)
Case study	Magnetotail	$F_2/F_1 < 10$	Øieroset et al. (2002)
Case study	Magnetotail	$F_2/F_1 < 10$	Fu et al. (2011)
Case study	Magnetotail	$F_2/F_1 < 10$	Ashour-Abdalla et al. (2011)
Case study	Magnetotail	$F_2/F_1 < 10$	Fu et al. (2013a)
Case study	Magnetotail	$F_2/F_1 < 10$	Huang et al. (2012)
Case study	Magnetotail	$F_2/F_1 < 20$	Hoshino et al. (2001)
Case study	Magnetotail	$F_2/F_1 < 30$	Imada et al. (2007)
Case study	Magnetotail	$F_2/F_1 < 30$	Vaivads et al. (2011)
Case study	Magnetotail	$F_2/F_1 < 100$	Chen et al. (2008)
Case study	Magnetotail	$F_2/F_1 < 100$	Retinò et al. (2008)
Case study	Magnetotail	$F_2/F_1 < 100$	Egedal et al. (2012)
Case study	Magnetotail	$F_2/F_1 > 10000$	This study

Appendix A




Summary of electron acceleration in previous studies. As can be seen, in previous statistics, the flux enhancement is below 10 times; in previous case studies, the flux enhancement is below 100 times. Here F_2/F_1 is estimated using differential particle fluxes (or PSDs) of the 40–120 keV electrons (see Figures 3(d)–(e)). In such an energy range, spacecraft (Cluster & Geotail) usually had several measurement channels. However, in each channel, the value of F_2/F_1 is very similar, because electron acceleration in such an energy range is usually adiabatic.

Appendix B

Structure of reconnection front. In this event, the reconnection front was first detected by C3 and C4 (located earthward)

then by C1 (located tailward). This is due to the finger-like shape of the reconnection front. Theoretically, magnetic reconnection is three dimensional (Fu et al. 2015; Chen et al. 2018) and can generate outflows extending widely in the dawn-dusk direction (Zhou et al. 2017). The speed of this outflow is usually different along the dawn-dusk direction, because of the non-uniform obstruction in the downstream region (Fujimoto 2016). As a result, many flow channels are formed (see the cartoon in Figure 4). Such multiple flow channels have been widely reported in previous simulations (Pritchett & Coroniti 2010; Fujimoto 2016) and observations (Panov et al. 2012; Zhou et al. 2017). In this event, C3 and C4 may detect a fast flow channel, and C1 may detect a slow flow channel (see Figure 4). The measurements of flow velocities indeed support this conjecture: in this event, C4 observed flow velocity up to $V_x = 1200 \text{ km s}^{-1}$, while C1 observed flow velocity $V_x = 600 \text{ km s}^{-1}$ (see Figure 2(c)).

ORCID iDs

H. S. Fu  <https://orcid.org/0000-0002-4701-7219>
 Y. Xu  <https://orcid.org/0000-0003-1863-7280>
 Y. V. Khotyaintsev  <https://orcid.org/0000-0001-5550-3113>

References

- Angelopoulos, V., Baumjohann, W., Kennel, C. F., et al. 1992, *JGR*, **97**, 4027
 Angelopoulos, V., McFadden, J. P., Larson, D., et al. 2008, *Sci*, **321**, 931
 Angelopoulos, V., Runov, A., Zhou, X. Z., et al. 2013, *Sci*, **341**, 1478
 Ashour-Abdalla, M., El-Alaoui, M., Goldstein, M. L., et al. 2011, *NatPh*, **7**, 360
 Baumjohann, W., Paschmann, G., & Cattell, C. A. 1989, *JGR*, **94**, 6597
 Burch, J. L., Torbert, R. B., Phan, T. D., et al. 2016, *Sci*, **352**, 1189
 Cao, D., Fu, H. S., Cao, J. B., et al. 2017, *GeoRL*, **44**, 3954
 Cao, J., Ma, Y., Parks, G., et al. 2013, *JGRA*, **118**, 313
 Cao, J. B., Ma, Y. D., Parks, G., et al. 2006, *JGR*, **111**, A04206
 Chen, L. J., Bhattacharjee, A., Puhl-Quinn, P. A., et al. 2008, *NatPh*, **4**, 19
 Chen, X. H., Fu, H. S., Liu, C. M., et al. 2018, *ApJ*, **852**, 17
 Drake, J. F., Swisdak, M., Che, H., & Shay, M. A. 2006, *Natur*, **443**, 553
 Duan, A. Y., Cao, J. B., Dunlop, M., & Wang, Z. Q. 2014, *JGRA*, **119**, 8902
 Egedal, J., Daughton, W., & Le, A. 2012, *NatPh*, **8**, 321
 Egedal, J., Lê, A., Zhu, Y., et al. 2010, *GeoRL*, **37**, L10102
 Escoubet, C. P., Fehringer, M., & Goldstein, M. 2001, *AnGeo*, **19**, 1197
 Fu, H. S., Cao, J. B., Cully, C. M., et al. 2014, *JGRA*, **119**, 9089
 Fu, H. S., Cao, J. B., Khotyaintsev, Y. V., et al. 2013b, *GeoRL*, **40**, 6023
 Fu, H. S., Khotyaintsev, Y. V., André, M., & Vaivads, A. 2011, *GeoRL*, **38**, L16104
 Fu, H. S., Khotyaintsev, Y. V., Vaivads, A., et al. 2012a, *GeoRL*, **39**, L10101
 Fu, H. S., Khotyaintsev, Y. V., Vaivads, A., et al. 2012b, *JGR*, **117**, A12221
 Fu, H. S., Khotyaintsev, Y. V., Vaivads, A., et al. 2012c, *GeoRL*, **39**, L06105
 Fu, H. S., Khotyaintsev, Y. V., Vaivads, A., et al. 2013a, *NatPh*, **9**, 426
 Fu, H. S., Vaivads, A., Khotyaintsev, Y. V., et al. 2015, *JGRA*, **120**, 3758
 Fu, H. S., Vaivads, A., Khotyaintsev, Y. V., et al. 2017, *GeoRL*, **44**, 37
 Fu, X. R., Lu, Q. M., & Wang, S. 2006, *PhPl*, **13**, 012309
 Fujimoto, K. 2016, *GeoRL*, **43**, 10557
 Gabrielse, C., Harris, C., Angelopoulos, V., et al. 2016, *JGRA*, **121**, 9560
 Grigorenko, E. E., Kronberg, E. A., Daly, P. W., et al. 2016, *JGRA*, **121**, 9985
 Guo, F., Li, H., Daughton, W., & Liu, Y.-H. 2014, *PhRvL*, **113**, 155005
 Guo, F., Liu, Y.-H., Daughton, W., & Li, H. 2015, *ApJ*, **806**, 167
 Hoshino, M. 2012, *PhRvL*, **108**, 135003
 Hoshino, M., Mukai, T., Terasawa, T., & Shinohara, I. 2001, *JGR*, **106**, 25979
 Huang, S. Y., Vaivads, A., Khotyaintsev, Y. V., et al. 2012, *GeoRL*, **39**, L11103
 Imada, S., Nakamura, R., Daly, P. W., et al. 2007, *JGR*, **112**, A03202
 Ji, H., Yamada, M., Hsu, S., & Kulsrud, R. 1998, *PhRvL*, **30**, 3256
 Johnstone, A. D., Alsop, C., Burge, S., et al. 1997, *SSRv*, **79**, 351
 Li, X., Guo, F., Li, H., & Birn, J. 2018a, *ApJ*, **855**, 80
 Li, X., Guo, F., Li, H., & Li, S. 2018b, *ApJ*, **866**, 4
 Lin, R. P., Krucker, S., Hurford, G. J., et al. 2003, *ApJL*, **595**, L69
 Liu, C. M., Fu, H. S., Cao, D., et al. 2018a, *ApJ*, **860**, 128
 Liu, C. M., Fu, H. S., Cao, J. B., et al. 2017a, *GeoRL*, **44**, 10116
 Liu, C. M., Fu, H. S., Vaivads, A., et al. 2018b, *GeoRL*, **45**, 556
 Liu, C. M., Fu, H. S., Xu, Y., et al. 2017b, *JGRA*, **122**, 594
 Liu, C. M., Fu, H. S., Xu, Y., et al. 2018c, *GeoRL*, **45**, 4628
 Liu, C. M., Fu, H. S., Xu, Y., Cao, J. B., & Liu, W. L. 2017c, *GeoRL*, **44**, 6492
 Lu, S., Angelopoulos, V., & Fu, H. S. 2016, *JGRA*, **121**, 9483
 Matsumoto, Y., Amano, T., Kato, T. N., & Hoshino, M. 2015, *Sci*, **347**, 974
 Øieroset, M., Lin, R. P., Phan, T. D., et al. 2002, *PhRvL*, **89**, 195001
 Panov, E. V., Sergeev, V. A., Pritchett, P. L., et al. 2012, *GeoRL*, **39**, L08110
 Peng, F. Z., Fu, H. S., Cao, J. B., et al. 2017, *JGRA*, **122**, 6349
 Phan, T. D., Eastwood, J. P., Shay, M. A., et al. 2018, *Natur*, **557**, 202
 Pritchett, P. L. 2006, *JGR*, **111**, A10212
 Pritchett, P. L., & Coroniti, F. V. 2010, *JGR*, **115**, A06301
 Retinò, A., Nakamura, R., Vaivads, A., et al. 2008, *JGR*, **113**, A12215
 Retinò, A., Sundkvist, D., Vaivads, A., et al. 2007, *NatPh*, **3**, 235
 Thorne, R. M., Li, W., Ni, B., et al. 2013, *Natur*, **504**, 411
 Vaivads, A., Retinò, A., Khotyaintsev, Y. V., & Andre, M. 2011, *AnGeo*, **29**, 1917
 Wang, J., Cao, J. B., Fu, H. S., et al. 2017, *JGRA*, **122**, 185
 Wang, R., Lu, Q., Li, X., et al. 2010, *JGR*, **115**, A11201
 Wei, X. H., Cao, J. B., Zhou, G. C., et al. 2007, *JGR*, **112**, A10225
 Wilken, B., Axford, W. I., Daglis, I., et al. 1997, *SSRv*, **79**, 399
 Wu, M. Y., Lu, Q. M., Volwerk, M., et al. 2013, *JGRA*, **118**, 4804
 Xu, Y., Fu, H. S., Liu, C. M., & Wang, T. Y. 2018a, *ApJ*, **853**, 11
 Xu, Y., Fu, H. S., Norgren, C., Hwang, K.-J., & Liu, C. M. 2018b, *PhPI*, **25**, 072123
 Yang, J., Cao, J. B., Fu, H. S., et al. 2017, *JGRA*, **122**, 4299
 Zhou, M., Ashour-Abdalla, M., Deng, X., et al. 2017, *JGRA*, **122**, 9513
 Zhou, M., Li, T., Deng, X., et al. 2016, *JGRA*, **121**, 3108